Energy & Environmental Science

Accepted Manuscript

ROYAL SOCIETY OF CHEMISTRY

www.rsc.org/ees

Journal Name

COMMUNICATION

Ni_2P as a Janus catalyst for water splitting: the oxygen evolution activity of Ni_2P nanoparticles

Received 00th January 20xx,
Accepted 00th January 20xx

DOI: 10.1039/x0xx00000x

www.rsc.org/

Lucas-Alexandre Stern,[†] Ligang Feng,[†] Fang Song, and Xile Hu*

Electrochemical water splitting into hydrogen and oxygen is a promising method for solar energy storage. The development of efficient electrocatalysts for water splitting has drawn much attention. However, catalysts that are active for both the hydrogen evolution and oxygen evolution reactions are rare. Herein, we show for the first time that nickel phosphide (Ni_2P), an excellent hydrogen evolving catalyst, is also highly active for oxygen evolution. A current density of 10 mA cm^{-2} is generated at an overpotential of only 290 mV in 1 M KOH. The high activity is attributed to the core-shell (Ni_2P/NiO_X) structure that the material adopts under catalytic conditions. The Ni_2P nanoparticles can serve as both cathode and anode catalysts for an alkaline electrolyzer, which generates 10 mA cm^{-2} at 1.63 V.

The water splitting reaction provides a convenient chemical method for renewable energy storage.[1] The two half reactions of water splitting, the hydrogen evolution reaction (HER: $2H^+ + 2e^- \rightarrow H_2$) and the oxygen evolution reaction (OER: $2H_2O \rightarrow O_2 + 4H^+ + 4e^-$), both require electrocatalysts to take place in a practical rate. The development of new and efficient water splitting catalysts, particularly those based on Earth-abundant elements, is an active area of energy research.[2-6] While significant progress has been made in this area, there are until now very few catalysts that are capable of catalyzing both HER and OER in the same media.[7-11] Such bifunctional, Janus catalysts might be attractive for a water splitting device because the integration of only one rather than two catalysts need to be considered.[7, 10] Artero and co-workers recently reported a Janus Co-based electrocatalyst material for water splitting in pH 7 phosphate buffer.[7] At reductive potentials, the resting catalyst is a Co oxo hydroxo phosphate species that catalyzes HER; at oxidative potentials, the resting catalyst is the well-known Co-Pi that catalyzes OER.[12] The switching of catalyst activity is enabled by the transformation of morphology and composition of the catalyst surface. Analogous behavior was reported by Wu and co-workers for amorphous Ni oxo hydroxo film in pH 9.2 borate buffer.[8] Grätzel and co-workers showed that NiFe layered double hydroxide is a bifunctional catalyst for water splitting in alkaline conditions, and applied it for water photolysis in conjunction with a perovskite tandem solar cell.[10] Herein, we show for the first time that Ni_2P, which has recently emerged as a new and highly efficient HER catalyst,[13, 14] can catalyze OER in alkaline medium with remarkable activity. Under catalytic conditions, we observe the *in-situ* formation of a core-shell Ni_2P/NiO_x assembly. The Ni_2P/NiO_x catalyst gives a current density of 10 mA cm^{-2} at overpotential of 290 mV, ranking among the most active non-precious OER catalysts. The activity of Ni_2P in both HER and OER allowed a construction of an efficient alkaline electrolyzer using only this bifunctional catalyst.

The Ni_2P nanoparticles were synthesized by two different methods. Polydispersed nanoparticles could be prepared by a simple thermal reaction of NaH_2PO_2 and $NiCl_2 \cdot 6H_2O$ at 250 °C.[14] The resulting Ni_2P particles have an averaged particle size of about 50 nm and are coated with a thin amorphous layer (Fig. 1a).

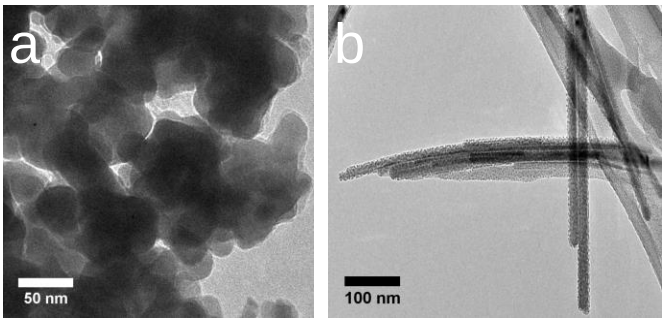

Fig. 1 (a) Transmission electron microscopy (TEM) image of polydispersed Ni_2P nanoparticles. (b) TEM image of Ni_2P nanowires.

[a] *L.-A. Stern, Dr. L.G. Feng, Dr. F. Song, Prof. Dr. X. L. Hu*
Laboratory of Inorganic Synthesis and Catalysis
Institute of Chemical Sciences and Engineering
École Polytechnique Fédérale de Lausanne (EPFL)
ISIC-LSCI, BCH 3305, 1015 Lausanne (Switzerland)
E-mail: xile.hu@epfl.ch
Homepage: http://lsci.epfl.ch.
† L.-A. Stern and L.G. Feng contributed equally to this work.
Electronic Supplementary Information (ESI) available: [details of any supplementary information available should be included here]. See DOI: 10.1039/x0xx00000x

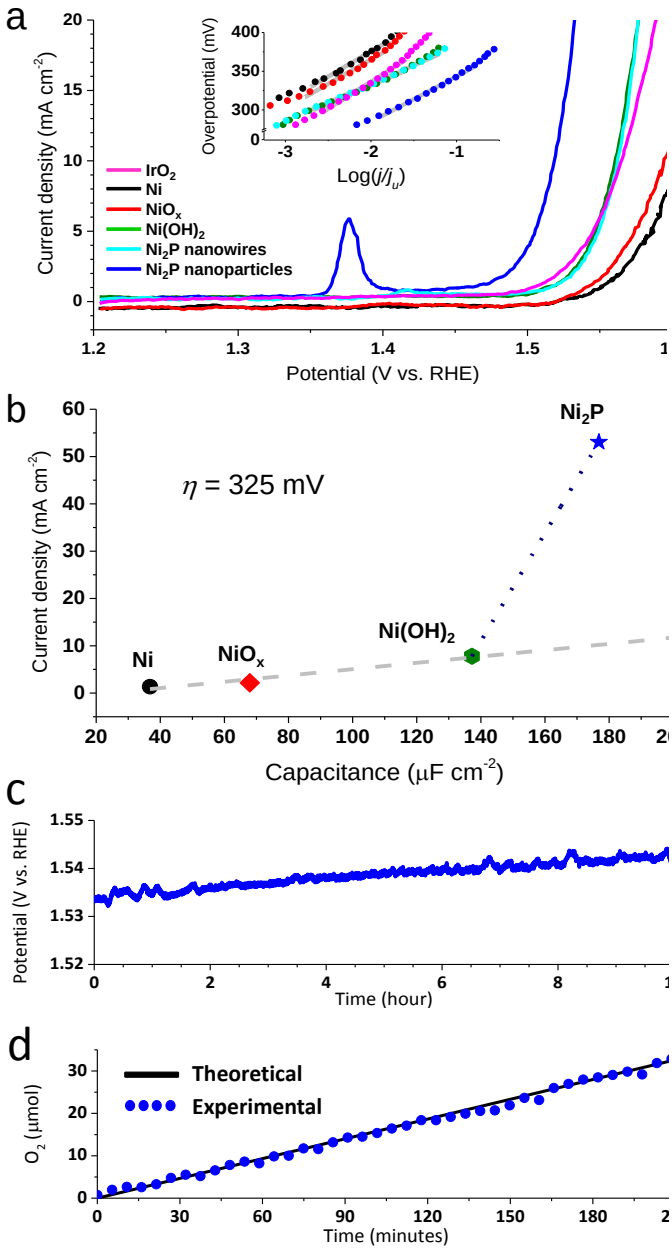

Fig. 2 (a) Linear sweep voltammetric (LSV) curves of Ni_2P nanomaterials, Ni nanoparticles, NiO nanoparticles, electrodeposited $Ni(OH)_2$, and IrO_2 in 1 M KOH. Inset: Tafel plots of the OER activity. (b) Correlation of electrocatalytic activity, namely, the current density at overpotential of 325 mV, with electrochemical capacitance of the different nickel materials. (c) Galvanostatic electrolysis on the Ni_2P nanoparticles in 1 M KOH at a constant current density of 10 mA cm^{-2} over 10 hours. (d) Faradaic efficiency of the OER catalyzed by Ni_2P in 1 M KOH at a current density of 14 mA cm^{-2}. The theoretical line represents the amount of O_2 expected for a 100% Faraday efficiency. Conditions: pretreated working electrode, pre-activated Ni_2P catalysts, 5 mV s^{-1}, 0.14 mg cm^{-2}.

More uniformly distributed Ni_2P nanowires could be prepared by heating nickel(II) acetylacetonate in a solution of oleic acid, trioctylamine, and tri-n-octylphosphine at 320 °C (*Caution: the reaction is pyrolytic and needs to be conducted under strictly inert atmosphere*).[15] These Ni_2P nanowires have an averaged width of about 11 nm and are covered of an amorphous surfactant layer (Fig. 1b). Further characterization of both types of Ni_2P nanoparticles can be found in the supplementary information (Fig. S1 and S2).

The OER activity of Ni_2P nanoparticles was evaluated using glassy carbon (GC) as the supporting electrode. Prior to measurements, the GC was pretreated electrochemically by repetitive cyclic voltammetry from 0.5 to 1.9 V *vs.* RHE in 1 M KOH. As described earlier, this pretreatment creates oxygenated surface functional groups and increases the hydrophilicity and wettability of the surface.[16] The Ni_2P catalysts were loaded onto the pretreated GC electrode by simple drop casting; a loading of 0.14 mg cm^{-2} was applied. 25 cycles of cyclic voltammetric scans (1.20 - 1.65 V *vs*. RHE) were used to activate the Ni_2P catalysts. Fig. 2a shows the linear sweep voltammograms (LSV) of Ni_2P in 1 M KOH at a potential window relevant to OER. For comparison, the activity of nanoparticles of IrO_2, Ni, NiO and an electrochemically synthesized $Ni(OH)_2$ film was also measured. A same loading of 0.14 mg cm^{-2} was applied on pretreated GC electrode for IrO_2, Ni, NiO nanoparticles. Characterization of the Ni and NiO can be found in the supplementary information (Fig. S3 and S4, ESI). The polydispersed Ni_2P nanoparticles are the most active catalyst. The overpotential to generate 10 mA cm^{-2} is only 290 mV. Ni_2P nanowires, IrO_2, and $Ni(OH)_2$ have similar activity, and the overpotential to generate 10 mA cm^{-2} is 330 mV. Ni and NiO nanoparticles are least active, requiring more than 365 mV of overpotential to generate 10 mA cm^{-2}. The different activity of the two types of Ni_2P is likely due to the presence of an amorphous layer of surfactant on the surface of the Ni_2P nanowires (Fig. 1b), which might limit the OER activity. Indeed, upon annealing of the nanowires to remove the surface organic impurities,[13] Ni_2P nanowires exhibit a similar OER activity as the polydispersed Ni_2P nanoparticles (Fig. S5). The Tafel slopes are 47 mV dec^{-1} for Ni_2P nanowires and $Ni(OH)_2$, 59 mV dec^{-1} for polydispersed Ni_2P nanoparticles, 65 mV dec^{-1} for Ni and NiO, and 70 mV dec^{-1} for IrO_2. Because the synthetic procedure for the polydispersed Ni_2P nanoparticles is simpler, safer, and higher yielding than that for the monodispersed Ni_2P nanowires, the former material was selected for further catalytic tests and characterization.

The electrocatalytic activity of a material often depends on the surface area. To make a better comparison of the activity of different nickel-based materials described here, their double layer capacitance, proportional to their electrochemical surface areas, were measured (Table 1). The Ni_2P nanoparticles indeed have a higher surface area under the same loading. Nevertheless, the increase in surface area is not the sole factor for its high activity. Fig. 2b shows that for Ni, NiO, and $Ni(OH)_2$, there is a linear correlation of the activity and capacitance. However, the activity of Ni_2P is significantly higher than predicted by this correlation.

The stability of the Ni_2P catalyst in OER was tested in galvanostatic electrolysis at 10 mA cm^{-2}. Fig. 2c shows that the overpotential merely increased 10 mV during 10 h of continuous operation. This indicates a good level of stability. The Faraday efficiency of OER was monitored during a galvanostatic electrolysis of 210 min. Fig. 2d shows that the amount of oxygen evolved corresponds to a quantitative Faraday yield.

Table 1 Comparison of OER activities of metal oxide catalysts in alkaline conditions

Material	Loading [mg cm^{-2}]	C_{dl} [μF cm^{-2}]	η@10 mA cm^{-2} [mV]	Ref.
Ni	0.14	36.8	377	This work
NiO	0.14	68	364	This work
$Ni(OH)_2$	0.14	137.2	331	This work
Ni_2P	0.14	176.9	290	This work
NiO_x	0.02	-	360	(19)
α-$Ni(OH)_2$	0.20	-	331	(20)
β-$Ni(OH)_2$	0.20	-	444	(20)
$NiCo_2O_4$	0.53	-	565	(21)
NiFe-LDH	0.20	-	320	(22)
CoO_x@CN	0.42	-	410	(11)
BSCF82	0.25	-	320	(24)
IrO_2	-	-	320	(18)
IrO_2[a]	0.35	-	275	(26)

[a] OER activity measured in acidic medium

The OER activity of Ni_2P is compared to some state-of-the-art catalysts (Table 1). Ni_2P is more efficient than the best nanostructured nickel oxides and $NiCo_2O_4$ spinel catalysts.[17-21] It is more active than NiFe-layered double hydroxide (NiFe-LDH) [22 22 2222] and cobalt-cobalt oxide/N-doped carbon hybrids (CoO_x@CN),[11] which require higher catalyst loadings and higher overpotential than Ni_2P to reach 10 mA cm^{-2} under similar operating conditions. Recently, the perovskite $Ba_{0.5}Sr_{0.5}Co_{0.8}Fe_{0.2}O_{3-\delta}$ (BSCF82) was reported as a highly active OER catalyst.[23] Ni_2P is also more active than BSCF82, having an overpotential that is 30 mV lower than the latter to reach 10 mA cm^{-2}.[24] While high surface area IrO_2 and its alloys are excellent OER catalysts, especially in acidic solutions,[25, 26] thin films of conventional IrO_2 nanoparticles on flat electrodes generally have η@10 mA cm^{-2} of more than 300 mV in alkaline solutions.[18] As shown in Fig. 2, Ni_2P is more active than such IrO_2 nanoparticles under these conditions.

Structural modification of Ni_2P during catalysis was probed by high-resolution TEM (HRTEM) (Fig. 3 and S6) and X-ray photoelectron spectroscopy (XPS) measurements (Fig. S7). After OER catalysis at 1.5 V for 1 h, the composition of Ni_2P nanoparticles changed significantly. HRTEM images show that numerous small nanoparticles with an average size of 2 – 3 nm are formed around the Ni_2P particles after oxygen evolution (Fig. 3). The ultrafine nanoparticles exhibit fringes indicative of registry order, or crystallinity (Fig. 3a). Fast Fourier transform (FFT) of the nanoparticles in the outer layer confirmed the crystallinity of these particles (Fig. 3a inset). The spacing of the fringes is characteristic to specific facets of nickel oxides/hydroxides species. On the other hand, the core material remains Ni_2P, indicated by the fringes corresponding to the <100> facet of Ni_2P (Fig. 3a). The distribution of different elements in the Ni_2P nanoparticles after OER was revealed by energy dispersive X-ray (EDX) elemental maps (Fig. 3b – e). The core-shell Ni_2P/NiO_x composition could be clearly seen (Fig. 3e). Nickel is homogeneously present in all particles (Fig. 3b), phosphorus is dominant in the inner layer (Fig. 3d), while oxygen is limited to the outer layer particles (Fig. 3c). This core-shell composition was further confirmed by XPS data.

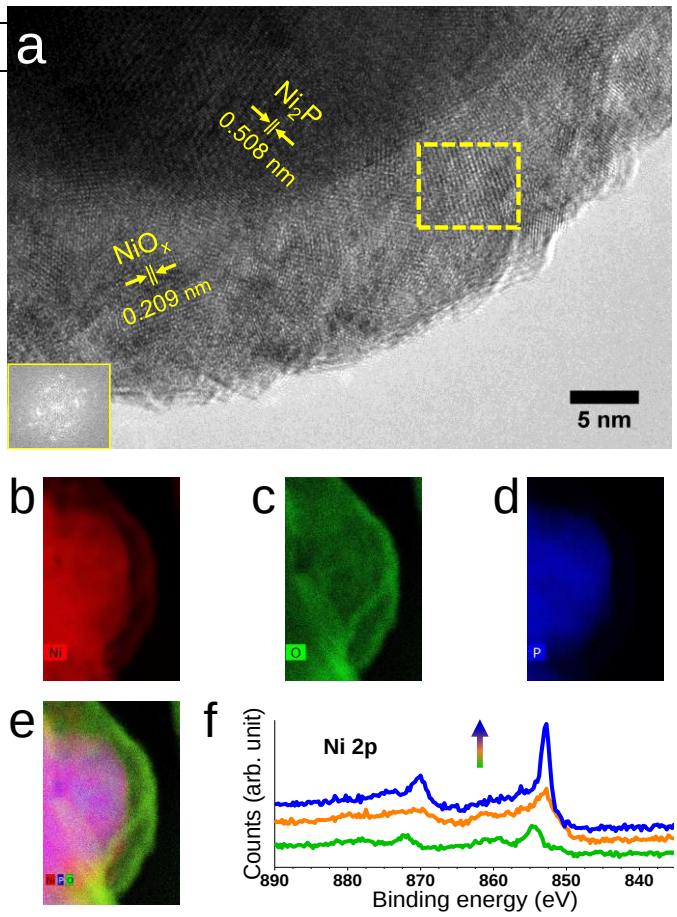

Fig. 3 (a) HRTEM image of the Ni_2P nanoparticles after electrochemical pretreatment at 1.5 V *vs.* RHE for one hour. Inset (lower left): FFT of the framed area (middle). The spots observed on the FFT are indicative of registry order and so of crystallinity. The lattice fringes spacing of the materials were determined using FFT. They correspond to the characteristic <100> facet of Ni_2P and specific facets of nickel oxides/hydroxides species, NiO_x. (b) – (e) Corresponding EDX maps of the elements on the sample region shown in (a). (b) Nickel elemental mapping. (c) Oxygen elemental mapping. (d) Phosphorus elemental mapping. (e) Combined elemental mapping of Ni, O, and P. (f) High-resolution depth-profiling XPS spectra of the Ni 2p area. As the profiling depth increases (arrow direction), the FWHM decreases, indicative of stronger metallic Ni content. This confirms the presence of a surface oxide layer around metallic nickel phosphide core.

After sputtering, the XPS survey spectra show lower oxygen and higher nickel contents (Fig. S7a and b). High resolution XPS depth profiling spectra of Ni 2p (Fig. 3f) show that as the sputtering depth increases the FWHM of the corresponding peak decreases and the nickel content increases, characteristic of nickel species with stronger metallic character. The corresponding binding energy is attributed to nickel phosphide.[27] The XPS data is, thus, consistent with a nickel phosphide core beneath a less conductive NiO_x surface. For the same reason, increase of the phosphorus content and decrease of the oxygen content was observed along a sputtering depth of 50 nm (Fig. S7d and e). The formation of the core-shell assembly was further confirmed by electrochemical measurements. The oxidation peak at 1.38 V *vs.* RHE in the LSV curves of Ni_2P (Fig. 2a) is characteristic of

the Ni(II)/Ni(III) oxidation in many Ni oxide/hydroxide and $NiFeO_x$ OER catalysts.[16, 17, 20, 27] We suspect the pre-activation process lead to the fabrication of the Ni_2P/NiO_x core-shell heterostructure. The observed increase in catalytic activity is then attributed to the formation of a stable core-shell assembly (Fig. S8). HRTEM images before OER revealed a metal-free oxygen-rich thin layer surrounding Ni_2P particles before OER (Fig. S9). Phosphorus was detected in this layer, suggesting that the layer might be composed of residual P_2O_5. The absence of nickel (Fig. S9c) in the amorphous layer prior to OER indicates that the core-shell Ni_2P/NiO_x assembly is generated *in-situ* under catalytic conditions on Ni_2P nanoparticles surface. These results are in agreement with XPS data (Fig. S10).[28] High-resolution XPS depth-profiling spectra of Ni 2p, O 1s, and P 2p using argon ion sputtering further confirm the composition of the as-prepared Ni_2P (Fig. S10c - e).

The higher activity of the Ni_2P/NiO_x heterostructure compared to other NiO_x and $Ni(OH)_2$ based catalysts warrants an explanation.[17, 20, 27] We hypothesize that the unique properties of the Ni_2P/NiO_x core-shell assembly facilitate catalytic OER. The Ni_2P core might play a significant role as conducting support in providing an effective electron pathway to the NiO_x shell.[29-31] Consistent with this hypothesis, the Ni_2P nanoparticles are much more active than NiO_x nanoparticles of similar size, after normalization of surface areas (Fig 2a and b). The Ni_2P core might be the perfect template to grow these particular NiO_x nanoparticles, which are more active than other forms of NiO_x. Indeed, for the same loading, the Ni_2P/NiO_x assemblies have the highest surface areas. Finally, synergistic effects might exist between the Ni_2P core and the NiO_x shell,[29, 30] which requires further study for confirmation.

Trace amount of iron incorporation was recently shown to be essential for the high OER activity of NiO_x- and $Ni(OH)_2$-based catalysts.[31] Moreover, the iron impurities present in commercial grade KOH was an adequate source for iron incorporation.[31] As the Ni_2P/NiO_x catalyst described here has a catalytically active NiO_x component, it is expected that iron incorporation also occurs during pre-activation in KOH. Indeed, the presence of a trace amount of iron at the surface of the Ni_2P/NiO_x catalyst after OER was confirmed by EDX (Fig. S11a). Moreover, if the iron impurities were removed from the electrolyte, then the Ni_2P/NiO_x requires 120 mV more in overpotential to reach 10 mA cm^{-2} (Fig. S11b). Thus, in the active form, the NiO_x shell is doped with Fe ions, similar to other NiO_x and $Ni(OH)_2$ materials.

Recently Ni_2P was shown to have high HER activity.[13, 14] The high OER activity of Ni_2P revealed here suggests that Ni_2P can serve as a bifunctional catalyst in water splitting. Fig. S12 shows the HER activity of the polydispered Ni_2P nanoparticles (1.8 mg cm^{-2}) in 1 M KOH. The overpotential is about 220 mV for 10 mA cm^{-2}, which is consistent with the previous report. An alkaline electrolyzer was then constructed using Ni_2P as the catalyst for both HER and OER. A loading of 5 mg cm^{-2} was applied on Ni foam supports. The cathode was used as it is, while the anode was activated by 10 cyclic voltammetric scans (from 1.1 to 1.8 V).

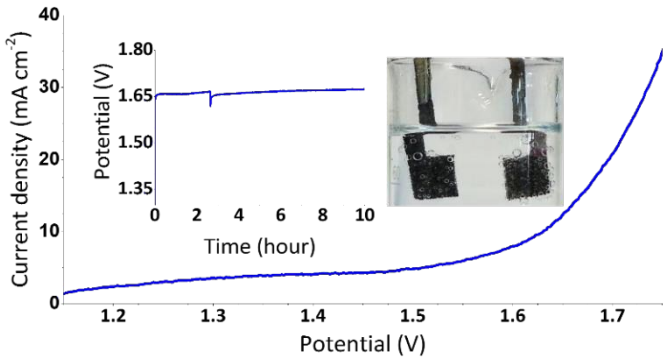

Fig. 4 Current-potential response of an alkaline electrolyzer using Ni_2P as catalyst for both OER and HER. Support: Ni foam; loading of catalyst: 5 mg cm^{-2}; electrolyte: 1 M KOH. At about 2.5 h, bubbles were mechanically removed from the electrode. Inset: galvanostatic electrolysis in 1 M KOH at a constant current density of 10 mA cm^{-2} over 10 hours. Photograph of the system showing the oxygen (left) and hydrogen (right) generation during water electrolysis

Fig 4 shows the current-potential response of this electrolyzer (in a 2-electrode setting). A current density of 10 mA cm^{-2} was obtained at about 1.63 V, which represents a combined overpotential of only about 400 mV for HER and OER. The potential was stable at this value during a 10 h galvanostatic electrolysis experiment using this electrolyzer (Fig. 4 inset). The Faraday yield of the alkaline electrolyzer was measured (Fig. S13), showing a quantitative Faraday yield for water splitting. When a glass frit was used to separate the HER and OER reaction chambers, a similar performance was obtained (Fig. S14). Thus, Ni_2P shows excellent bifunctional activity and stability in water splitting. As a reference, water splitting using Ni foam required a combined overpotential of 560 mV for 10 mA cm^{-2}.

The NiO_x layer of the core-shell Ni_2P-NiO_x catalyst might be removed to generate clean Ni_2P by prolonged electrolysis in acidic solutions at reductive potentials. After oxide removal, the Ni_2P nanoparticles is highly active for HER in acid, generating 10 mA cm^{-2} at η = 136 mV (Fig. S15), comparable to the reported activity of this catalyst.

Conclusions

In summary, we show for the first time that Ni_2P is capable of catalyzing OER in alkaline conditions. The active form of the catalyst for OER is a core-shell Ni_2P/NiO_x assembly generated *in-situ* under catalytic conditions. The OER activity is superior to some state of the art catalysts, having an η@10 mA cm^{-2} of only 290 mV. The bifunctional activity of Ni_2P enabled the construction of an alkaline water electrolyzer using Ni_2P as catalyst for both HER and OER. This electrolyzer splits water with a current density of 10 mA cm^{-2} at 1.63 V. These findings highlight the potential of Ni_2P as cathode and anode catalysts of future (photo)electrochemical water splitting devices.

Acknowledgement

This work is supported by the EPFL.

Notes and references

1. N. S. Lewis and D. G. Nocera, *Proc. Natl. Acad. Sci. USA*, 2006, 103, 15729-15735.
2. M. G. Walter, E. L. Warren, J. R. McKone, S. W. Boettcher, Q. X. Mi, E. A. Santori and N. S. Lewis, *Chem. Rev.*, 2010, 110, 6446-6473.
3. T. R. Cook, D. K. Dogutan, S. Y. Reece, Y. Surendranath, T. S. Teets and D. G. Nocera, *Chem. Rev.*, 2010, 110, 6474-6502.
4. M. S. Faber and S. Jin, *Energy Environ. Sci.*, 2014, 7, 3519-3542.
5. H. Dau, C. Limberg, T. Reier, M. Risch, S. Roggan and P. Strasser, *Chemcatchem*, 2010, 2, 724-761.
6. A. Singh and L. Spiccia, *Coord. Chem. Rev.*, 2013, 257, 2607-2622.
7. S. Cobo, J. Heidkamp, P.-A. Jacques, J. Fize, V. Fourmond, L. Guetaz, B. Jousselme, V. Ivanova, H. Dau, S. Palacin, M. Fontecave and V. Artero, *Nat. Mater.*, 2012, 11, 802-807.
8. C. He, X. Wu and Z. He, *J. Phys. Chem. C*, 2014, 118, 4578-4584.
9. X. Liu, H. Zheng, Z. Sun, A. Han and P. Du, *ACS Catal.*, 2015, 5, 1530–1538.
10. J. Luo, J.-H. Im, M. T. Mayer, M. Schreier, M. K. Nazeeruddin, N.-G. Park, S. D. Tilley, H. J. Fan and M. Graetzel, *Science*, 2014, 345, 1593-1596.
11. H. Jin, J. Wang, D. Su, Z. Wei, Z. Pang and Y. Wang, *J. Am. Chem. Soc.*, 2015, 137, 2688-2694.
12. M. W. Kanan, Y. Surendranath and D. G. Nocera, *Chem. Soc. Rev.*, 2009, 38, 109-114.
13. E. J. Popczun, J. R. McKone, C. G. Read, A. J. Biacchi, A. M. Wiltrout, N. S. Lewis and R. E. Schaak, *J. Am. Chem. Soc.*, 2013, 135, 9267-9270.
14. L. Feng, H. Vrubel, M. Bensimon and X. Hu, *Phys. Chem. Chem. Phys.*, 2014, 16, 5917-5921.
15. Y. Chen, H. She, X. Luo, G.-H. Yue and D.-L. Peng, *Journal of Crystal Growth*, 2009, 311, 1229-1233.
16. L.-A. Stern and X. Hu, *Faraday Discuss.*, 2014, 176, 363-379.
17. L. Trotochaud, J. K. Ranney, K. N. Williams and S. W. Boettcher, *J. Am. Chem. Soc.*, 2012, 134, 17253-17261.
18. C. C. L. McCrory, S. H. Jung, J. C. Peters and T. F. Jaramillo, *J. Am. Chem. Soc.*, 2013, 135, 16977-16987.
19. K. Fominykh, J. M. Feckl, J. Sicklinger, M. Doeblinger, S. Boecklein, J. Ziegler, L. Peter, J. Rathousky, E.-W. Scheidt, T. Bein and D. Fattakhova-Rohlfing, *Adv. Funct. Mater.*, 2014, 24, 3123-3129.
20. M. Gao, W. Sheng, Z. Zhuang, Q. Fang, S. Gu, J. Jiang and Y. Yan, *J. Am. Chem. Soc.*, 2014, 136, 7077-7084.
21. H. Shi and G. Zhao, *J. Phys. Chem. C*, 2014, 118, 25939-25946.
22. M. Gong, Y. G. Li, H. L. Wang, Y. Y. Liang, J. Z. Wu, J. G. Zhou, J. Wang, T. Regier, F. Wei and H. J. Dai, *J. Am. Chem. Soc.*, 2013, 135, 8452-8455.
23. J. Suntivich, K. J. May, H. A. Gasteiger, J. B. Goodenough and Y. Shao-Horn, *Science*, 2011, 334, 1383-1385.
24. K. J. May, C. E. Carlton, K. A. Stoerzinger, M. Risch, J. Suntivich, Y.-L. Lee, A. Grimaud and Y. Shao-Horn, *J. Phys. Chem. Lett.*, 2012, 3, 3264-3270.
25. S. Park, Y. Shao, J. Liu and Y. Wang, *Energy Environ. Sci.*, 2012, 5, 9331-9344.
26. L. Ouattara, S. Fierro, O. Frey, M. Koudelka and C. Comninellis, *J. Appl. Electrochem.*, 2009, 39, 1361-1367.
27. R. L. Doyle, I. J. Godwin, M. P. Brandon and M. E. G. Lyons, *Phys. Chem. Chem. Phys.*, 2013, 15, 13737-13783.
28. P. E. R. Blanchard, A. P. Grosvenor, R. G. Cavell and A. Mar, *J. Mater. Chem.*, 2009, 19, 6015-6022.
29. M. Gong, W. Zhou, M.-C. Tsai, J. Zhou, M. Guan, M.-C. Lin, B. Zhang, Y. Hu, D.-Y. Wang, J. Yang, S. J. Pennycook, B.-J. Hwang and H. Dai, *Nat. Commun.*, 2014, 5, 4695.
30. G. Elmaci, C. E. Frey, P. Kurz and B. Zumreoglu-Karan, *Inorg. Chem.*, 2015, 54, 2734-2741.
31. L. Trotochaud, S. L. Young, J. K. Ranney and S. W. Boettcher, *J. Am. Chem. Soc.*, 2014, 136, 6744-6753.